A New Model for the Planetary Radiation Pressure Acceleration for Optical Solar Sails

Carzana, L.; Visser, P.N.A.M.; Heiligers, M.J.

Citation (APA)
Carzana, L., Visser, P. N. A. M., & Heiligers, M. J. (2023). A New Model for the Planetary Radiation Pressure Acceleration for Optical Solar Sails. In *Proceedings of the 6th International Symposium on Space Sailing: New York, USA, 5-9 June 2023*

Important note
To cite this publication, please use the final published version (if applicable).
Please check the document version above.

A New Model for the Planetary Radiation Pressure Acceleration for Optical Solar Sails

Livio Carzana[a,*], Pieter Visser[a], Jeannette Heiligers[a]

[a]Faculty of Aerospace Engineering, Delft University of Technology, 2329 HS, Delft, The Netherlands

Abstract

Solar sailing is a propellantless propulsion method that exploits solar radiation pressure to generate thrust. In recent years, several solar sails have been launched into Earth-bound orbit to demonstrate this technology's potential. Because planetary radiation pressure can reach magnitudes comparable to that of solar radiation pressure in proximity of the Earth, it cannot automatically be neglected in near-Earth solar-sail mission design studies. Nevertheless, its effect on the solar-sail dynamics has been investigated only to a very limited, first-order extent, and every study considered an "ideal" – i.e., perfectly reflecting – sail model. Although employing the ideal sail model proves useful for preliminary orbital analyses, its limited fidelity prevents more in-depth research into the near-Earth solar-sail dynamics and trajectory optimization. In light of this, this paper provides a new planetary radiation pressure acceleration model for optical solar sails. This model forms an extension of the "spherical" planetary radiation pressure acceleration model for ideal solar sails devised by Carzana et al. in Reference [1]. In the current paper, the underlying assumptions and full derivation of the newly devised optical model are presented. Subsequently, the accuracy of the optical model is analyzed through a comparison with the ideal model, using NASA's upcoming ACS3 mission as reference scenario.

Keywords: solar sail, dynamical model, Earth-bound, planetary radiation pressure, optical sail model, ACS3 mission

1. Introduction

Solar sailing is a propulsion method that uses solar radiation as main source of thrust [2]. Due to its propellantless nature and mission-enabling potential for a wide variety of applications [3, 4], solar sailing has drawn increasingly more attention in the scientific community over the last decades. As a result, a number of technology demonstration missions have been launched, both in the interplanetary and near-Earth environments. Among the most recent missions are, for example, NASA's NEA Scout and Gama's Gama Alpha missions. Even more missions are scheduled for the near future, such as NASA's Advanced Composite Solar Sail System (ACS3) and Gama's Beta missions [5]. Most of these sailcraft have flown (or are planned to fly) in low-Earth orbit [6], where several perturbations can affect the solar-sail dynamics, including gravitational perturbations, eclipses, atmospheric drag, and planetary radiation pressure (PRP). While a number of studies have been conducted on the dynamics and trajectory optimization of drag-perturbed solar sails [7, 8, 9], the effects of PRP on the sailcraft dynamics and control have been

investigated only to a very limited, first-order extent. Studying the effects of PRP on the solar-sail dynamics is relevant because, for some orbital scenarios, PRP can achieve a non-trivial intensity, with magnitudes of up to 20% of the solar radiation pressure (SRP) [1]. However, determining the PRP acceleration accurately presents several difficulties, mainly related to the models used to represent the Earth's radiation and the optical properties of the solar sail. For this reason, early studies on this topic considered simplistic models. These studies characterized the PRP acceleration in proximity of the Earth [10] and investigated the optimization of PRP-perturbed sailcraft trajectories [11]. In these studies the sail is assumed to be ideal – that is, it is perfectly reflecting – while the Earth is approximated as a uniform bright disk, as per the finite-disk radiation model devised by McInnes [2]. As an extension of McInnes' finite-disk model, the so-called "spherical" radiation model has been developed in the work by Carzana [1], where a thorough investigation of the achievable blackbody and albedo radiation pressure accelerations experienced by sailcraft in close proximity of the Earth has been conducted. The analytical model derived in Ref. [1] considers the Earth as a spherical, uniform radiation source,

whose brightness depends on the sailcraft altitude, latitude, and Sun-Earth-sailcraft angle. Although the spherical radiation model derived in Ref. [1] allows for more accurate results than the finite-disk model, it still assumes the sail to behave as an ideal, perfect reflector. Generally, the use of the ideal sail model leads to useful results for first-order analyses. For more in-depth analyses, the so-called optical sail model is often preferred [2]. This model accounts for the absorptivity, reflectivity, and emissivity properties of the sail and has been used extensively to model the SRP acceleration in several works, see the overview in Ref. [12]. A similar optical model for the PRP acceleration has not been found in available literature and, similar to the optical model for the SRP acceleration, would aid in increasing the fidelity of the solar-sail dynamics. In light of this, this paper aims to bridge this gap of knowledge by providing a new PRP acceleration model valid for optical solar sails and assuming a spherical Earth radiative model. As such, this model forms an extension of the spherical PRP acceleration model for ideal solar sails devised by Carzana in Ref. [1].
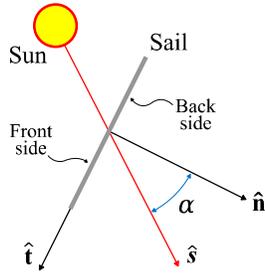

Fig. 1. Solar-sail pitch angle, α, normal direction, $\hat{n}$, and SRP transversal direction, $\hat{t}$.

2. Dynamical Model

The equations of motion of a solar sail in Earth-bound orbit are expressed in an inertial Earth-centered reference frame, $\mathcal{S}(x, y, z)$. In this frame, the x-axis points towards the vernal equinox, the z-axis is perpendicular to the equatorial plane and points towards the north pole, and the y-axis completes the right-handed frame. Within this frame, the equations of motion of a flat-shaped solar sail under the influence of Earth's central gravity, SRP and PRP can be expressed in vectorial form as:

$$\ddot{r} + \frac{\mu}{r^3} r = a_{SRP} + a_{PRP} \qquad (1)$$

where $\mu = 398600.4415 \ \text{km}^3\text{s}^{-2}$ is the Earth's gravitational parameter [13], $r = [x, y, z]^T$ is the sailcraft position vector, $r = \|r\|$, a_{SRP} is the SRP acceleration, and

a_{PRP} is the PRP acceleration. These accelerations will be described in more detail in the following sections.

2.1. Solar Radiation Pressure Acceleration

The SRP acceleration is defined using the optical sail model, which accounts for the absorption, reflection, and emission properties of the solar sail. When this model is employed, the SRP acceleration is given by [2]:

$$a_{SRP} = a_{SRP,n} + a_{SRP,t} \qquad (2)$$

where $a_{SRP,n}$ and $a_{SRP,t}$ are the normal and transversal components of the SRP acceleration, respectively. The former is directed along the sail normal direction with no component pointing towards the Sun, $\hat{n}$, while the latter points in the SRP transversal direction, $\hat{t}$, tangential to the sail plane, see Fig. 1. The SRP transversal direction can be defined from $\hat{n}$ and the direction of sunlight, $\hat{s}$, as follows:

$$\hat{t} = \hat{n} \times \frac{(\hat{s} \times \hat{n})}{\|\hat{s} \times \hat{n}\|} \qquad (3)$$

The acceleration components $a_{SRP,n}$ and $a_{SRP,t}$ are defined as [2]:

$$a_{SRP,n} = v \frac{a_c}{2} \left\{ \left(1 + \tilde{r}_f s_f\right) \cos^2(\alpha) \right.$$
$$+ \left(1 - s_f\right) \tilde{r}_f B_f \cos(\alpha) \qquad (4)$$
$$\left. + \left(1 - \tilde{r}_f\right) \frac{\varepsilon_f B_f - \varepsilon_b B_b}{\varepsilon_f + \varepsilon_b} \cos(\alpha) \right\} \hat{n}$$

$$a_{SRP,t} = v \frac{a_c}{2} \left(1 - \tilde{r}_f s_f\right) \cos(\alpha) \sin(\alpha) \ \hat{t} \qquad (5)$$

where $\alpha \in [0, \pi/2]$ represents the solar-sail pitch angle measured between $\hat{s}$ and $\hat{n}$, see again Fig. 1, and $v \in [0,1]$ is the shadow factor, which accounts for the effect of eclipses and ranges from 0 (no sunlight reaches the sail) to 1 (sail completely illuminated). In this paper, eclipses are modeled with a conical shadow model similar to the one presented in Ref. [14, 15], with the only difference that $v = 0$ both when in umbra and penumbra. The solar-sail characteristic acceleration, a_c, represents the maximum SRP acceleration (achieved for $\alpha = 0$) at a distance of 1 AU from the Sun and is defined as [2]:

$$a_c = \frac{2\mathbb{S}_\oplus}{c\sigma} \qquad (6)$$

where $\mathbb{S}_\oplus = 1367 \ \text{W/m}^2$ is the solar flux at Earth [13], $c = 299792.458 \ \text{km/s}$ is the speed of light in vacuum [16], and σ is the sailcraft mass-to-sail area ratio. Finally, the optical properties of the sail are specified

through the parameters $\tilde{r}$, s, B, and ε, which represent the reflectivity, specular reflection coefficient, non-Lambertian reflection coefficient, and emissivity of the sail, respectively, with the subscript *"f"* indicating that the optical coefficient refers to the sail front side and the subscript *"b"* is used to refer to the sail back side. It should be noted that Eqs. (4) and (5) are based on the assumption that only the sail front side is exposed to sunlight and, conversely, the sail back side is never illuminated. Because of this, the normal and transversal components of the SRP acceleration do not depend on the reflectivity and specular reflection coefficient of the sail back side, $\tilde{r}_b$ and s_b. As explained in the next section, this assumption does not hold for the PRP acceleration, as planetary radiation can illuminate both sides of the sail, thus requiring the knowledge of $\tilde{r}_b$ and s_b.

2.2. Planetary Radiation Pressure Acceleration

To determine the PRP acceleration exerted on a solar sail, knowledge of the amount of planetary radiation received by the sail, its corresponding flux and radiation pressure is required. The mathematical derivation to determine these quantities is provided in Ref. [1] and is reported here for the sake of completeness.

If an elementary piece of Earth's surface dA is considered, see Fig. 2a, the amount of power irradiated in a generic direction $\hat{l}$ and enclosed within an infinitesimal solid angle $d\Omega$ is represented by the second differential d^2P as [17]:

$$d^2P = I \cos(\vartheta) d\Omega dA \qquad (7)$$

where I represents the planetary radiation intensity (across the entire electromagnetic spectrum) along the normal direction to dA, $\hat{N}$, and $\vartheta \in [0, \pi/2]$ is the angle between $\hat{N}$ and $\hat{l}$, see again Fig. 2a. Assuming Earth's surface to be a Lambertian scatterer, the radiation intensity can be expressed as [18]:

$$I = \frac{S}{\pi} \qquad (8)$$

where S is the planetary radiation power flux (i.e., the emitted radiation power per unit area) at the surface element, dA. When only the radiation received by the solar sail is considered, $d\Omega$ represents the solid angle subtended by an infinitesimal piece of illuminated sail surface, dA_{sail}. In this case, $d\Omega$ is defined as [19]:

$$d\Omega = \frac{dA_{sail} \cos(\theta)}{l^2} \qquad (9)$$

where $\theta \in [0, \pi/2]$ is the angle between $\hat{l}$ and the sail normal direction pointing away from dA, $\hat{n}_{ill}$, and l is

the magnitude of the vector l pointing from dA to dA_{sail}, see Figs. 2a and 2b. Making use of Eqs. (8) and (9), Eq. (7) can be rewritten as:

$$d^2P = \frac{S}{\pi} \frac{\cos(\vartheta) \cos(\theta)}{l^2} dA_{sail} dA \qquad (10)$$
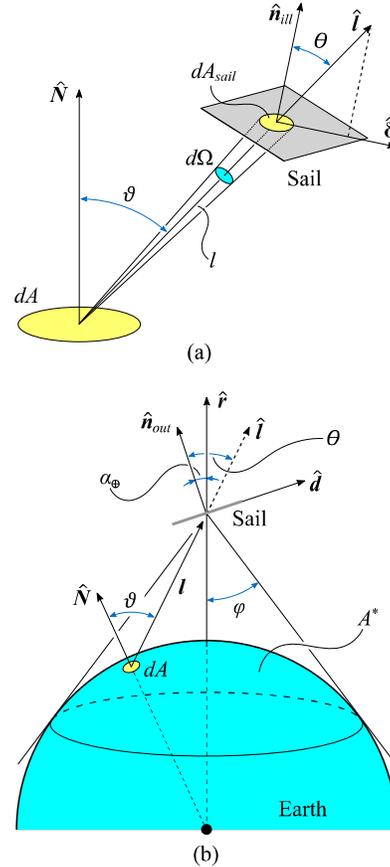

(a)

(b)

Fig. 2. Geometry of the problem to determine the PRP acceleration exerted on a solar sail.

Since this paper considers a flat-shaped solar sail whose dimensions are significantly smaller than l, θ and l can be assumed to be constant across the entire sail surface. This assumption allows to easily integrate Eq. (10) with respect to dA_{sail} over the entire sail surface, A_{sail}. Performing the integration yields the radiation power dP received by the entire sail due to the radiation emitted by dA:

$$dP = \frac{S}{\pi} \frac{\cos(\vartheta) \cos(\theta)}{s^2} A_{sail} dA \qquad (11)$$

The power flux at the sail's location due to the radiation emitted by dA, dS_{sail}, is then found as:

$$dS_{sail} = \frac{dP}{A_{sail}\cos(\theta)} = \frac{S}{\pi}\frac{\cos(\vartheta)}{l^2}dA \qquad (12)$$

so that the corresponding radiation pressure $d\mathbb{P}$ is given by [2]:

$$d\mathbb{P} = \frac{dS_{sail}}{c} = \frac{S}{\pi c}\frac{\cos(\vartheta)}{l^2}dA \qquad (13)$$

Equation (13) allows to determine the acceleration exerted on the sail due to the radiation emitted by the surface element dA, $d\boldsymbol{a}_{PRP}$. Indeed, by taking into account the optical properties of the sail, $d\boldsymbol{a}_{PRP}$ can be defined in a similar fashion to the SRP acceleration as:

$$d\boldsymbol{a}_{PRP} = d\boldsymbol{a}_{PRP,n} + d\boldsymbol{a}_{PRP,\delta} \qquad (14)$$

where the normal and transversal components of the infinitesimal PRP acceleration, $d\boldsymbol{a}_{PRP,n}$ and $d\boldsymbol{a}_{PRP,\delta}$, respectively, are given by:

$$\begin{aligned}
d\boldsymbol{a}_{PRP,n} = \frac{d\mathbb{P}}{\sigma}\Big\{ &\big(1+\tilde{r}_{ill}s_{ill}\big)\cos^2(\theta)\hat{\boldsymbol{n}}_{ill} \\
&+\big(1-s_{ill}\big)\tilde{r}_{ill}B_{ill}\cos(\theta)\hat{\boldsymbol{n}}_{ill} \\
&+\big(1-\tilde{r}_{ill}\big)\frac{\varepsilon_f B_f - \varepsilon_b B_b}{\varepsilon_f + \varepsilon_b}\cos(\theta)\hat{\boldsymbol{n}}\Big\} \\
= \frac{S}{\pi c\sigma}\Big\{ &\big(1+\tilde{r}_{ill}s_{ill}\big)\frac{\cos(\vartheta)\cos^2(\theta)}{l^2}\hat{\boldsymbol{n}}_{ill} \\
&+\big(1-s_{ill}\big)\tilde{r}_{ill}B_{ill}\frac{\cos(\vartheta)\cos(\theta)}{l^2}\hat{\boldsymbol{n}}_{ill} \\
&+\big(1-\tilde{r}_{ill}\big)\frac{\varepsilon_f B_f - \varepsilon_b B_b}{\varepsilon_f + \varepsilon_b}\frac{\cos(\vartheta)\cos(\theta)}{l^2}\hat{\boldsymbol{n}}\Big\}dA
\end{aligned} \qquad (15)$$

$$\begin{aligned}
d\boldsymbol{a}_{PRP,\delta} &= \frac{d\mathbb{P}}{\sigma}\big(1-\tilde{r}_{ill}s_{ill}\big)\cos(\theta)\sin(\theta)\,\hat{\boldsymbol{\delta}} \\
&= \frac{S}{\pi c\sigma}\big(1-\tilde{r}_{ill}s_{ill}\big)\frac{\cos(\vartheta)\cos(\theta)\sin(\theta)}{l^2}\hat{\boldsymbol{\delta}}\,dA
\end{aligned} \qquad (16)$$

In the above equations, the subscript *"ill"* is used to refer to the optical coefficients of the sail side illuminated by the radiation emitted by the surface element dA, while $\hat{\boldsymbol{\delta}}$ represents the PRP transversal direction relative to dA, which can be found from Eq. (3) by substituting $\hat{\boldsymbol{\delta}}$ for $\hat{\boldsymbol{t}}$ and $\hat{\boldsymbol{l}}$ for $\hat{\boldsymbol{s}}$, see Fig. 2a.

Although the decomposition of $d\boldsymbol{a}_{PRP}$ into its normal and transversal components is similar to that performed in Eq. (2) for the SRP acceleration, it should be noted that a major difference exists, which is due to the different definitions of the SRP transversal direction, $\hat{\boldsymbol{t}}$, and PRP transversal direction relative to dA, $\hat{\boldsymbol{\delta}}$. Indeed, while $\hat{\boldsymbol{t}}$ is uniquely defined for a given sail attitude, $\hat{\boldsymbol{\delta}}$ is not, as its direction depends on the specific surface element dA considered and it can point anywhere within the sail plane. When this dependency of $\hat{\boldsymbol{\delta}}$ on

dA is taken into account, Eq. (14) can be integrated over the entire visible surface of the Earth as seen from the sailcraft, A^*, hence yielding the total PRP acceleration exerted on the solar sail, i.e.:

$$\boldsymbol{a}_{PRP} = \int_{A^*} d\boldsymbol{a}_{PRP} = \int_{A^*} \big(d\boldsymbol{a}_{PRP,n} + d\boldsymbol{a}_{PRP,\delta}\big) \qquad (17)$$

The solution to the PRP acceleration integral in Eq. (17) depends on the Earth-sail geometrical configuration and, most importantly, on how the planetary flux, S, varies across the visible surface A^*. Because the planetary flux varies geographically following a complex pattern, no general closed-form analytical solution to the acceleration integral exists. To circumvent this problem, in the literature the PRP acceleration integral is usually solved numerically by discretizing the visible surface A^* and making use of maps providing the geographical distribution of the Earth's blackbody radiation flux and albedo coefficient. Such numerical methods enable a high accuracy which, however, comes at the cost of a large computational effort. Therefore, in this paper an analytical approach is pursued instead, which assumes a constant planetary flux S over the entire visible surface A^*. To compute this value of S, the previously mentioned maps are used to approximate the Earth's blackbody radiation flux and albedo coefficient as sinusoidal functions of latitude. Then, by performing a surface average, a constant, analytical value of S is found. For more information on the definition of the surface-averaged planetary radiation flux, the reader is referred to Ref. [1].

Considering a constant planetary flux allows to analytically solve the PRP acceleration integral in Eq. (17), yielding to:

$$\begin{aligned}
\boldsymbol{a}_{PRP} = \frac{S}{c\sigma}\Big\{ &\frac{2}{3}\Big[\big(1+\tilde{r}_{in}s_{in}\big)G_{FNS,in} - \big(1+\tilde{r}_{out}s_{out}\big)G_{FNS,out}\Big]\hat{\boldsymbol{n}}_{out} \\
&+\Big[\big(1-s_{in}\big)\tilde{r}_{in}B_{in}G_{FND,in} - \big(1-s_{out}\big)\tilde{r}_{out}B_{out}G_{FND,out}\Big]\hat{\boldsymbol{n}}_{out} \\
&+\frac{\varepsilon_f B_f - \varepsilon_b B_b}{\varepsilon_f + \varepsilon_b}\Big[\big(1-\tilde{r}_{in}\big)G_{FND,in} + \big(1-\tilde{r}_{out}\big)G_{FND,out}\Big]\hat{\boldsymbol{n}} \\
&+\frac{2}{3\pi}\Big[\big(1-\tilde{r}_{in}s_{in}\big)G_{FT,in} + \big(1-\tilde{r}_{out}s_{out}\big)G_{FT,out}\Big]\hat{\boldsymbol{d}}\Big\}
\end{aligned} \qquad (18)$$

where $\hat{\boldsymbol{d}}$ is the PRP transversal direction relative to the Earth displayed in Fig. 2b, found from Eq. (3) by substituting $\hat{\boldsymbol{d}}$ for $\hat{\boldsymbol{t}}$ and the radial direction, $\hat{\boldsymbol{r}}$, for $\hat{\boldsymbol{s}}$. G_{FNS}, G_{FND}, and G_{FT} represent the normal specular, normal diffuse, and transversal geometrical factors, respectively, while the subscripts *"in"* and *"out"* indicate if the optical coefficients and geometrical factors refer to the inward or outward side of the sail with respect to the Earth. This differentiation is required because for

particular sail orientations planetary radiation can illuminate both the inward and outward sides of the sail, therefore contributing to $\boldsymbol{a}_{PRP}$. The geometrical factors are all defined in the range [0,1] and they correlate the Earth-sail geometrical configuration to the different components of the PRP acceleration. By indicating the regions of the surface A^* that are visible from the inward and outward sides of the sail by A_{in}^* and A_{out}^*, the geometrical factors can be defined as follows:

$$G_{FNS,\diamond} = \frac{3}{2\pi} \int_{A_\diamond} \frac{\cos(\vartheta)\cos^2(\theta)}{l^2} dA \qquad (19)$$

$$G_{FND,\diamond} = \frac{1}{\pi} \int_{A_\diamond} \frac{\cos(\vartheta)\cos(\theta)}{l^2} dA \qquad (20)$$

$$G_{FT,\diamond} = \frac{3}{2} \int_{A_\diamond} \frac{\cos(\vartheta)\cos(\theta)\sin(\theta)}{l^2} dA \qquad (21)$$

where the symbol $"\diamond"$ has been used as placeholder to indicate either the subscript "in" or "out".

The solutions to the surface integrals on the right-hand side of Eq. (19)-(21) depend on the geometrical configuration of the sail with respect to the Earth, which is uniquely defined by the orbital radius, r, planetary cone angle (PCA), $\alpha_\oplus \in [0, \pi/2]$, and maximum view angle, $\varphi \in [0, \pi/2]$, see Fig. 2b. The PCA is defined as the angle between $\hat{\boldsymbol{n}}_{out}$ and $\hat{\boldsymbol{r}}$ while φ represents the angle between the direction pointing to the Earth's tangent as seen from the sailcraft and $-\hat{\boldsymbol{r}}$. The full analytical solution to the geometrical factor integrals is presented in the following subsections.

2.2.1. Normal Specular Geometrical Factor

Depending on the sail orientation with respect to the Earth, two possible configurations can be identified:

a) If $\alpha_\oplus + \varphi \le \pi/2$, the incoming radiation from the visible surface A^* illuminates only the inward side of the sail. In this case, the outward geometrical factor is $G_{FNS,out} = 0$, while the inward geometrical factor, $G_{FNS,in}$, is given by Eq. (22), where $H = R/r$ is the adimensional inverse orbital radius, $R = 6378.1363$ km is the Earth radius [13], and:

$$A = \frac{\cos(\alpha_\oplus)}{\sin(\alpha_\oplus)}\sqrt{\frac{1}{H^2} - 1} \quad ; \quad B = \sqrt{\frac{H^2}{\cos^2(\alpha_\oplus)} - 1}$$

b) If $\alpha_\oplus + \varphi > \pi/2$, both sail sides are illuminated and the inward and outward geometrical factors are given by Eqs. (23) and (24).

2.2.2. Normal Diffuse Geometrical Factor

The normal diffuse geometrical factors correspond to the view factors of the sail sides with respect to the Earth. Their expressions were found by F.G. Cunningham in Ref. [19] and are reported hereinafter for completeness:

a) If $\alpha_\oplus + \varphi \le \pi/2$, $G_{FND,in}$ is given by Eq. (25) and $G_{FND,out} = 0$.

b) If $\alpha_\oplus + \varphi > \pi/2$, $G_{FND,in}$ and $G_{FND,out}$ are given by Eqs. (26) and (27), respectively.

$$G_{FNS,in}\left(H,\alpha_\oplus\right) = 1 - \sqrt{1-H^2}\left[1 - H^2\left(1 - \frac{3}{2}\sin^2(\alpha_\oplus)\right)\right] \qquad (22)$$

$$G_{FNS,in}\left(H,\alpha_\oplus\right) = 1 - \frac{1}{\pi}\left\{\frac{1}{2}\sqrt{1-H^2}\left[H^2\left(1-3\cos^2(\alpha_\oplus)\right)+2\right]\cos^{-1}(-A)+\tan^{-1}(B)-\frac{3}{2}B^3\cos^4(\alpha_\oplus)-\frac{1}{2}B\cos^2(\alpha_\oplus)\left(3\cos^2(\alpha_\oplus)-1\right)\right\} \qquad (23)$$

$$G_{FNS,out}\left(H,\alpha_\oplus\right) = \frac{1}{\pi}\left\{-\frac{1}{2}\sqrt{1-H^2}\left[H^2\left(1-3\cos^2(\alpha_\oplus)\right)+2\right]\cos^{-1}(A)+\tan^{-1}(B)-\frac{3}{2}B^3\cos^4(\alpha_\oplus)-\frac{1}{2}B\cos^2(\alpha_\oplus)\left(3\cos^2(\alpha_\oplus)-1\right)\right\} \qquad (24)$$

$$G_{FND,in}\left(H,\alpha_\oplus\right) = H^2\cos(\alpha_\oplus) \qquad (25)$$

$$G_{FND,in}\left(H,\alpha_\oplus\right) = \frac{1}{2} - \frac{1}{\pi}\left\{\sin^{-1}\left(\frac{H}{\sin(\alpha_\oplus)}\sqrt{\frac{1}{H^2}-1}\right) + B\cos(\alpha_\oplus)\sqrt{1-H^2} - H^2\cos(\alpha_\oplus)\cos^{-1}(-A)\right\} \qquad (26)$$

$$G_{FND,out}\left(H,\alpha_\oplus\right) = \frac{1}{2} - \frac{1}{\pi}\left\{\sin^{-1}\left(\frac{H}{\sin(\alpha_\oplus)}\sqrt{\frac{1}{H^2}-1}\right) + B\cos(\alpha_\oplus)\sqrt{1-H^2} + H^2\cos(\alpha_\oplus)\cos^{-1}(A)\right\} \qquad (27)$$

$$G_{FT,in}\left(H,\alpha_\oplus\right) = \frac{3\pi}{4}H^2\sqrt{1-H^2}\sin(2\alpha_\oplus) \qquad (28)$$

$$G_{FT,in}\left(H,\alpha_\oplus\right) = \frac{1}{2}\left\{B\left[2\sin(\alpha_\oplus)\cos^3(\alpha_\oplus)\left(B^2+2+\frac{\cos^2(\alpha_\oplus)}{\sin^2(\alpha_\oplus)}\right)-\left(1+H^2\right)\frac{\cos^3(\alpha_\oplus)}{\sin(\alpha_\oplus)}\right]+3H^2\sqrt{1-H^2}\sin(\alpha_\oplus)\cos(\alpha_\oplus)\cos^{-1}(-A)\right\} \qquad (29)$$

$$G_{FT,out}\left(H,\alpha_\oplus\right) = \frac{1}{2}\left\{B\sin(\alpha_\oplus)\cos^3(\alpha_\oplus)\left[B^2\left(2-\frac{\cos^2(\alpha_\oplus)}{\sin^2(\alpha_\oplus)}\right)+3\right]-3H^2\sqrt{1-H^2}\sin(\alpha_\oplus)\cos(\alpha_\oplus)\cos^{-1}(A)\right\} \qquad (30)$$

2.2.3. Transversal Geometrical Factor

Similar to the other geometrical factors, the definition of the transversal geometrical factor depends on whether both sides of the sail receive planetary radiation:

a) If $\alpha_\oplus + \varphi \leq \pi/2$, $G_{FT,in}$ is given by Eq. (28) and $G_{FT,out} = 0$.

b) If $\alpha_\oplus + \varphi > \pi/2$, $G_{FT,in}$ and $G_{FT,out}$ are given by Eqs. (29) and (30), respectively.

3. Accuracy Analysis

In this section, a parametric analysis is presented which aims to validate the optical PRP acceleration model presented in the previous section and quantify its accuracy compared to a high-fidelity numerical model. To achieve this, a wide variety of PRP perturbed, Earth-bound orbits have been propagated considering different models for the PRP acceleration, $\boldsymbol{a}_{PRP}$. These different models are:

a) NRTDM model. This numerical model computes the PRP acceleration by approximating the acceleration integral of Eq. (17) with a finite sum. This algorithm is implemented in NRTDM (Near Real-Time Density Model), a software tool developed at the Delft University of Technology under ESA contract [20, 21]. In order to model the planetary flux distribution across the Earth, this model makes use of two monthly averaged maps (one for the blackbody radiation flux and one for the albedo coefficient) obtained from the ANGARA software package developed by Hyperschall Technologie Göttingen GmbH [22]. Due to its numerical nature, this model allows to determine the PRP acceleration with a very high accuracy, although requiring a large computational effort. For more information on NRTDM, the reader is referred to [20].

b) Spherical PRP acceleration model for an optical solar sail, see Section 2.2. The sail optical coefficients employed have been taken from NASA's upcoming ACS3 solar-sail mission. The ACS3 sail membrane consists of a polymer film (polyethelene nepthalate) coated with an aluminum layer on the front side and a chromium layer on the back side [23]. The aluminum layer's optical coefficients are $\{\tilde{r}_f, s_f, B_f, \varepsilon_f\} = \{0.90, 0.74, 0.03, 0.79\}$, while the chromium layer's optical coefficients are $\{\tilde{r}_b, s_b, B_b, \varepsilon_b\} = \{0.43, 0.23, 0.60, 0.67\}^2$.

c) Spherical PRP acceleration model for an ideal solar sail. This model corresponds to the spherical PRP acceleration model devised by Carzana in Ref. [1] for ideal sails. It represents a special case of the optical PRP acceleration model presented in Section 2.2, found by considering the following "ideal" optical coefficients: $\{\tilde{r}_f, s_f, B_f, \varepsilon_f\} = \{1, 1, 2/3, 0\}$.

d) Model in which the PRP acceleration is neglected, i.e., $\boldsymbol{a}_{PRP} = \boldsymbol{0}$ at any time.

All analyses make use of the ACS3 mission orbit as baseline scenario, with a solar-sail characteristic acceleration of $a_c = 0.045$ mm/s² and the following vector of initial orbital elements defined in frame $\mathcal{S}(x, y, z)$:

$$[a_0, e_0, i_0, \text{LTAN}_0, \omega_0, f_0]^T =$$

$$\left[7093.1363 \text{ km}, 0, 98.2490 \text{ deg}, \begin{Bmatrix} 00{:}00\,\text{AM} \\ 00{:}30\,\text{AM} \\ \vdots \\ 11{:}30\,\text{AM} \end{Bmatrix}, 0 \text{ deg}, 0 \text{ deg} \right]^T \quad (31)$$

where a is the semi-major axis, e the eccentricity, i the inclination, ω the argument of perigee, f the true anomaly, LTAN stands for Local Time of the Ascending Node, and the subscript "0" denotes the initial value of these variables[3]. These orbital elements represent a circular, Sun-synchronous orbit with initial altitude $h_0 = a_0 - R = 715$ km. In Eq. (31), several values of the LTAN are considered, spaced by 0.5 hours along the entire 24-hour time span. This parameter defines the orbit orientation in frame $\mathcal{S}(x, y, z)$ and is equivalent to the right-ascension of the ascending node, which, in a similar fashion, is spaced by 7.5 deg across the entire 360-degree angular span. The parametric analysis also considers 12 different simulation start times, corresponding to the 15th day of each month of 2023. For each initial orbit, the solar-sail dynamics given in Eq. (1) are propagated while implementing locally optimal orbit-raising and inclination-changing steering laws. These steering laws are computed based on an algorithm similar to the one devised by McInnes for ideal sails [2], though adapted to the optical sail model presented in Section 2.1. It should be noted that because these steering laws account only for SRP in the optimization process, in the analyses, the PRP acceleration is considered as an uncontrolled perturbing acceleration affecting the orbit. For each initial orbit, each simulation start time and each steering law, four different propagations have been performed in which the PRP acceleration is computed through the four models listed above. Then, the relative errors between the final altitude/inclination obtained by

---

the NRTDM model (taken as the ground truth) and each of the analytical models, ε_{rel}, are computed. The parameter ε_{rel} is used as metric of the accuracy of the analytical models and its definition is given by:

$$\varepsilon_{rel} = \frac{\left| \text{œ}_{NRTDM,f} - \text{œ}_{An,f} \right|}{\text{œ}_{NRTDM,f} - \text{œ}_0} \quad (32)$$

where œ_0 indicates the initial value of the steering law's target parameter (i.e., h or i) and $\text{œ}_{NRTDM,f}$ and $\text{œ}_{An,f}$ represent the final values of the target parameter found through the NRTDM and the analytical model under consideration, respectively. For each simulation, the dynamics have been propagated for 10 days, using Matlab®'s *ode45* integrator with absolute and relative tolerances of 10^{-12}.

The top plot of Fig. 3 shows the variation of the relative error with the LTAN for the orbit-raising steering law for all analytical models. For each model, a band is displayed which represents the range of relative errors obtained by considering simulation start times at different months. All the error bands follow a 12-hour periodic trend, approximately symmetric with respect to the LTAN at 12AM. This is due to the relative orientations of the Sun-synchronous orbits with respect to the direction of sunlight, which can be similar even for different LTANs and therefore yield similar errors, ε_{rel}. All

models display small errors for an LTAN at 6AM/PM (corresponding to a dawn-dusk orbit), as in this case the PRP perturbs the orbit only to a very minor extent. On the other hand, when an LTAN at 12AM/PM is considered (corresponding to a noon-midnight orbit), the PRP acceleration is the largest and therefore the errors achieved, ε_{rel}, are maximal. As can be seen in the plot, neglecting the PRP acceleration in the dynamics yields large relative errors, even in the order of 12%. When employing the spherical ideal PRP model, these errors are strongly reduced, reaching values of 5% at most. Due to their higher fidelity with respect to the ideal PRP model, the optical PRP acceleration model achieves even smaller errors, in the range 0.2-1.1%. In addition to its increased accuracy, it is worth noting that the width of the optical PRP acceleration model's error band is smaller than the ideal model's error band, thus implying also a smaller error variation with the simulation start date.

The bottom plot of Fig. 3 displays the variation of ε_{rel} for the inclination-changing steering law, for different LTAN values and PRP acceleration models. In this case, a 12-hour periodicity in the errors is again obtained, although the error bands appear skewed and asymmetric, unlike the ones observed for the orbit-raising case (top plot of Fig. 3). This asymmetry is due to the complex, discontinuous nature of the inclination-
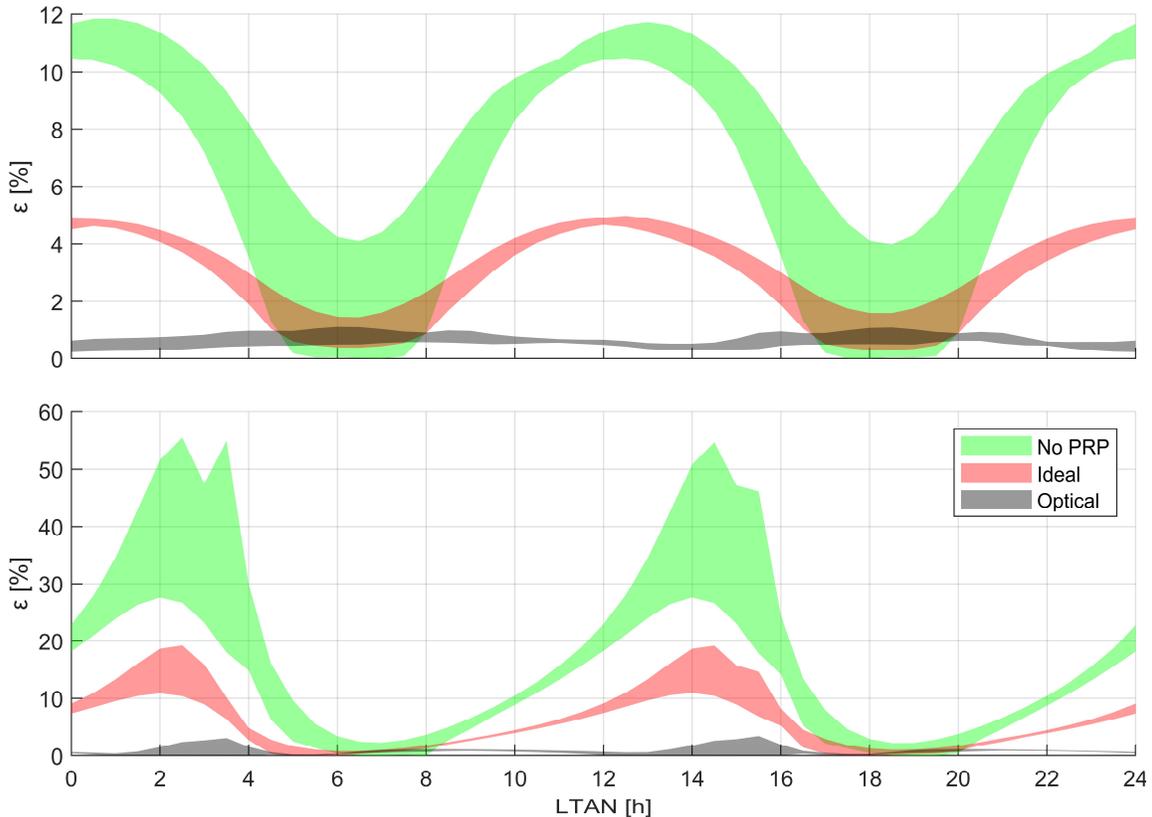

Fig. 3. Relative errors on the altitude increase (top) and inclination increase (bottom) of different PRP acceleration analytical models with respect to the NRTDM model.

changing steering law, for which orbits with similar orientations with respect to the sunlight direction still yield different increases in inclination. Similar to the orbit-raising case, all models achieve small errors for an LTAN around 6AM/PM, due to the small PRP acceleration achieved in this orbital scenario. Conversely, the largest errors are achieved for an LTAN approximately at 3AM/PM, as the PRP perturbation is maximal. The bottom plot of Fig. 3 shows that if the PRP acceleration is not accounted for in the dynamics, very large errors are produced, reaching magnitudes even in the order of 55%. When the PRP ideal acceleration model is employed, smaller errors are achieved, albeit still considerable: ε_{rel} reaches values up to 19.2%. On the other hand, significantly more limited errors are achieved when the PRP optical model is employed, as ε_{rel} reaches values of at most 3.4%. When comparing the error bands of the PRP ideal and optical acceleration models, it can again be noted that the former exhibits a wider spread than the latter, indicating that the optical model achieves a smaller error variation with the simulation start date.

4. Conclusions

This paper presented a new analytical model for planetary radiation pressure (PRP) acceleration, particular for optical solar sails. This model forms an extension of the "spherical" PRP acceleration model devised by Carzana for ideal (i.e., perfectly reflecting) solar sails [1]. A parametric analysis has been performed to quantify the model's accuracy compared to other PRP acceleration models. To this aim, the trajectory of NASA's upcoming ACS3 sailcraft has been propagated for a large set of initial orbital conditions, with the PRP acceleration either neglected or modeled through a high-fidelity numerical model, the newly devised optical model, or the pre-existent ideal model. The results show that employing the optical model yields a substantial increase in accuracy. Indeed, when an orbit-raising steering law is adopted, the maximum relative error in altitude increase of the optical model compared to the high-fidelity numerical model is in the order of 1.1%, whereas the relative error of the ideal model can reach values of 5%. Similarly, when an inclination-changing steering law is adopted, the optical PRP acceleration model attains a relative error of at most 3.4%, while the ideal model reaches a maximum value of 19.2%. Ultimately, the results also show that neglecting the PRP acceleration from the dynamics highly affects the results, as in that case the maximum relative errors on the altitude and inclination increases are 12% and 55%, respectively.

Acknowledgements

References

[1] L. Carzana, P. Visser and J. Heiligers, "A New Model for the Planetary Radiation Pressure Acceleration for Solar Sails," *under review at the Journal of Guidance, Control, and Dynamics,* 2023.

[2] C. R. McInnes, Solar Sailing - Technology, Dynamics and Mission Applications, Springer, 2004.

[3] D. A. Spencer, L. Johnson and A. C. Long, "Solar sailing technology challenges," *Aerospace Science and Technology,* vol. 93, 2019. DOI: 10.1016/j.ast.2019.07.009.

[4] M. Macdonald and C. R. McInnes, "Solar Sail Science Mission Applications and Advancement," *Advances in Space Research,* pp. 1702-1716, 2011. DOI: 10.1016/j.asr.2011.03.018.

[5] W. K. Wilkie, J. M. Fernandez, O. R. Stohlman and et al., "An Overview of the NASA Advanced Composite Solar Sail (ACS3) Technology Demonstration Project," *AIAA Scitech 2021 Forum,* 2021.

[6] M. Macdonald, Advances in Solar Sailing, Springer, 2014, pp. 95-113.

[7] L. Carzana, P. Visser and J. Heiligers, "Locally optimal control laws for Earth-bound solar sailing with atmospheric drag," *Aerospace Science and Technology,* vol. 127, no. 107666, 2022. DOI: 10.1016/j.ast.2022.107666.

[8] G. Mengali and A. A. Quarta, "Near-Optimal Solar-Sail Orbit-Raising from Low Earth Orbit," *Journal of Spacecraft and Rockets,* vol. 42, no. 5, pp. 954-958, 2005. DOI: 10.2514/1.14184.

[9] V. Stolbunov, M. Ceriotti, C. Colombo and C. R. McInnes, "Optimal Law for Inclination Change in an Atmosphere Through Solar Sailing," *Journal of Guidance, Control, and Dynamics,* vol. 36, no. 5, pp. 1310-1323, 2013. DOI: 10.2514/1.59931.

[10] A. De Iuliis, F. Ciampa, L. Felicetti and M. Ceriotti, "Sailing with Solar and Planetary Radiation Pressure," in *Proceedings of ISSS 2019: 5th International Symposium on Solar Sailing,* Aachen, Germany, 2019. DOI: 10.1016/j.asr.2019.11.036.

[11] A. Barles, M. Ceriotti, F. Ciampa and L. Felicetti, "An Optimal Steering Law for Sailing with Solar and Planetary Radiation Pressure," *Aerospace Science and Technology,* vol. 118, 2021. DOI: 10.1016/j.ast.2021.107051.

[12] B. Fu, E. Sperber and F. Eke, "Solar sail technology — A state of the art review," *Progress in Aerospace Sciences,* vol. 86, pp. 1-19, 2016.

[13] J. R. Wertz and W. J. Larson, Space Mission Analysis and Design, El Segundo: Microcosm Press and Dordrecht: Kluwer Academic Publishers, 2005.

[14] C. R. Ortiz Longo and S. L. Rickman, "Method for the Calculation of Spacecraft Umbra and Penumbra Shadow Terminator Points," NASA Center for AeroSpace Information, Linthicum Heights, 1995.

[15] P. Kelly and R. Bevilacqua, "An Optimized Analytical Solution for Geostationary Debris Removal using Solar Sails," *Acta Astronautica,* vol. 162, pp. 72-86, 2019. DOI: 10.1016/j.actaastro.2019.05.055.

[16] E. Tiesinga, P. J. Mohr, D. B. Newell and B. N. Taylor, "CODATA recommended values of the fundamental physical constants: 2018," *Reviews of Modern Physics,* vol. 93, 2021. DOI: 10.1103/RevModPhys.93.025010.

[17] B. W. Carroll and D. A. Ostlie, An Introduction to Modern Astrophysics, Cambridge, UK: Cambridge University Press, 2017. DOI: 10.1017/9781108380980.

[18] J. Lissauer and I. de Pater, Fundamental Planetary Science: Physics, Chemistry and Habitability, Cambridge, UK: Cambridge University Press, 2013.

[19] F. G. Cunningham, "Power Input to a Small Flat Plate from a Diffusely Radiating Sphere, with Application to Earth Satellites," National Aeronautics and Space Administration, Washington DC, 1961.

[20] E. Doornbos et al., "Algorithm Theoretical Basis Document," in *GOCE+ theme 3: Air density and wind retrieval using GOCE data, ESA contract 4000102847/NL/EL,* 2014.

[21] E. Doornbos, Thermospheric density and wind determination from satellite dynamics, Delft, The Netherlands: Springer, Berlin, Heidelberg, 2012.

[22] B. Fritsche et al., "Radiation pressure forces on complex spacecraft, final report, ESOC contract 11908," 1998.

[23] J. Ho Kang et al., "Durability characterization of mechanical interfaces in solar sail membrane structures," *Advances in Space Research,* vol. 67, no. 9, pp. 2643-2654, 2021.